

Phosphonated Trityl Probe for Concurrent *In vivo* Tissue Oxygen and pH Monitoring Using EPR-based Techniques

Ilirian Dhimitruka,[†] Andrey A. Bobko,[†] Timothy D. Eubank[†], Denis A. Komarov,[§] and Valery V.

Khramtsov^{†}*

[†]Dorothy M. Davis Heart & Lung Research Institute and Division of Pulmonary, Allergy, Critical Care & Sleep Medicine, Department of Internal Medicine, The Ohio State University, Columbus, OH 43210, United States

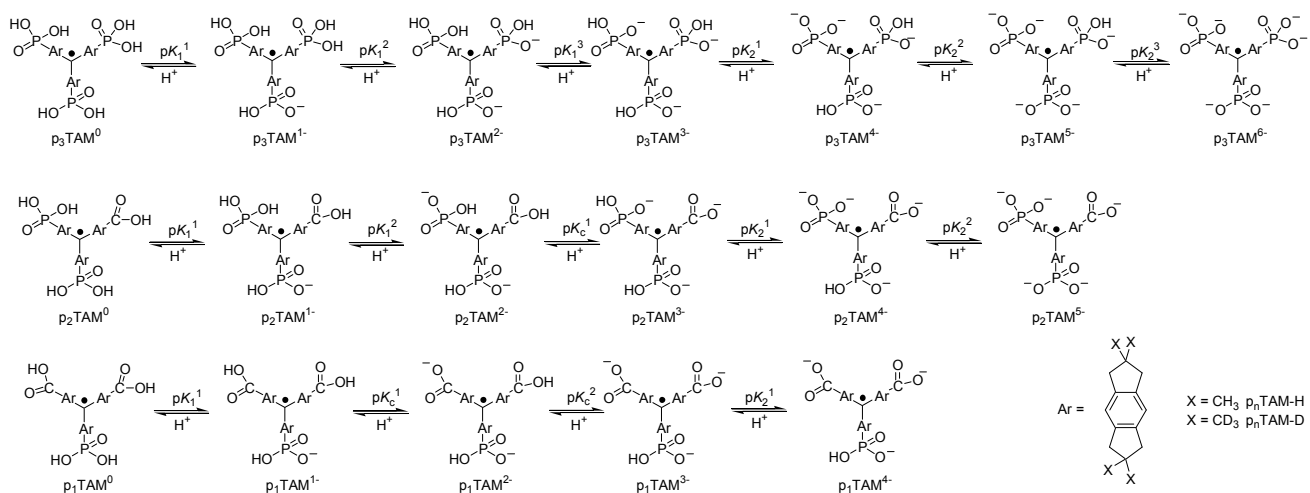
[§]Vorozhtsov Institute of Organic Chemistry, Novosibirsk 630090, Russia

valery.khramtsov@osumc.edu

Table of content:

1.	Acid-base equilibrium for p _n TAM probes	S2
2.	X-band EPR spectra of p ₁ TAM-H probe	S2
3.	X-band EPR spectra and titration curves of p ₂ TAM-H and p ₂ TAM-D	S3
4.	Spectral parameters and dissociation constants of p ₂ TAM-D	S4
5.	Concentration self-broadening of p ₁ TAM-D	S4
6.	Partition coefficients for p ₁ TAM-D probe	S4
7.	Acid-induced aggregation of p _n TAM-D and Finland TAM-D	S5
8.	An exemplified analysis of in vivo L-band EPR spectra of p ₁ TAM-D probe	S6
9.	Mass spectra of p ₁ TAM and p ₂ TAM probes	S7
10.	Literature cited	S10

Scheme S11. The scheme of acid-base equilibrium for p_n TAM trityl radicals. pK_1^i and pK_2^i denote the pK_a values of first and second ionization constants for each ($i = 1, 2, 3$) phosphonic acid residue; pK_c^i denote the pK_a values of ionization constants for each ($i = 1, 2$) carboxylic acid residue of p_n TAM probes.



X-band EPR spectra of p_1 TAM-H, p_2 TAM-H and p_2 TAM-D at different pH values and titration curves for p_2 TAM radicals

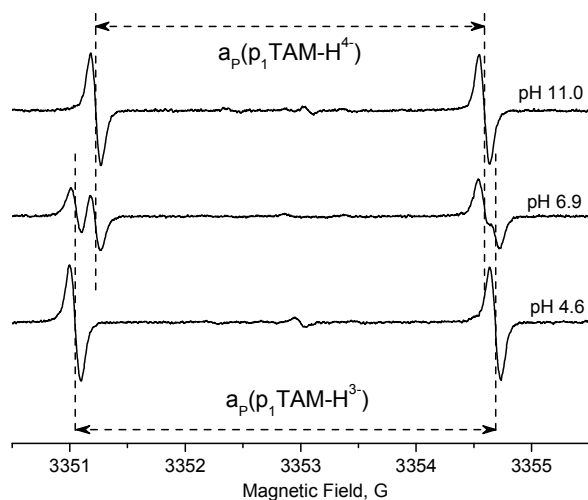


Figure S11. EPR spectra of 100 μ M p_1 TAM-H solutions in 1 mM Na-phosphate buffer, 150 mM NaCl, measured at various pH values under nitrogen atmosphere and temperature 37 °C. X-Band EPR spectrometer settings: microwave power, 130 μ W; time constant, 20.48 ms; conversion time, 5 ms; sweep time, 20.48 s; modulation frequency, 10 kHz; modulation amplitude, 0.05 G; sweep width 5.5 G; number of points, 4096.

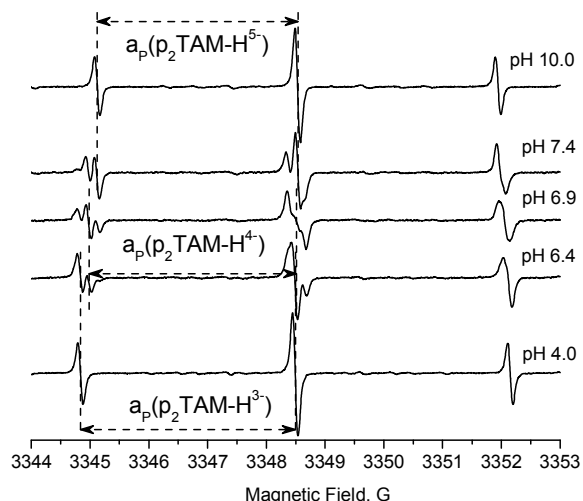


Figure SI2. X-band EPR spectra of 250 μM $p_2\text{TAM-H}$ solutions in 1 mM Na-phosphate buffer, 150 mM NaCl, measured at various pH values under nitrogen atmosphere and temperature 37 $^\circ\text{C}$. Spectrometer settings: microwave power, 130 μW ; time constant, 20.48 ms; conversion time, 5 ms; sweep time, 20.48 s; modulation frequency, 10 kHz; modulation amplitude, 0.05 G; sweep width 10 G; number of points, 4096.

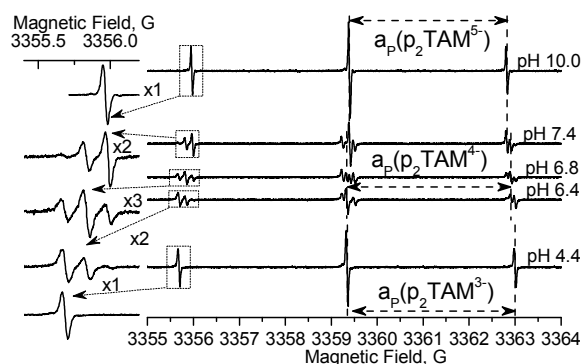


Figure SI3. X-band EPR spectra of 0.2 mM $p_2\text{TAM-D}$ solutions in 1 mM Na-phosphate buffer, 150 mM NaCl, measured at various pHs under nitrogen atmosphere, at 37 $^\circ\text{C}$. Spectrometer settings: microwave power, 40 μW ; modulation frequency, 10 kHz; modulation amplitude, 0.02 G; number of points, 8192.

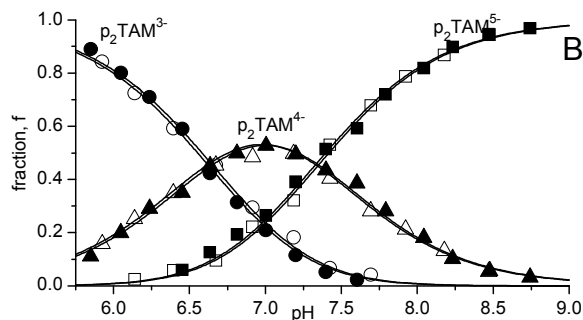


Figure SI4. The pH dependencies of fraction of the ionization states of diphosphonated $p_2\text{TAMs}$ calculated from the corresponding EPR spectra (Figs. SI2 and SI1-3). The closed and open symbols denote the data obtained for $p_2\text{TAM-D}$ and $p_2\text{TAM-H}$, correspondingly. The squares denote $p_2\text{TAM}^{5-}$, triangles denote $p_2\text{TAM}^{4-}$ and circles denote $p_2\text{TAM}^{3-}$ ionization states (See Scheme SI1). Solid lines represent the best fits using standard titration equations yielding pK_a values presented in the Table SI1.

Table SII. The pK_a Values and X-Band EPR Spectral Parameters for Different Ionization States of p_2 TAM-D.

Ionization State	pK_a	a_{p1} (PO_3^{2-}), mG	a_{p2} (HPO_3^-), mG	a_{p3} (H_2PO_3), mG	ΔH_{pp} , mG	Δg , mG
p_2 TAM $^{5-}$	7.35 ± 0.05	3420 ± 5 (2) ^a	Na	na	34 ± 2	0
p_2 TAM $^{4-}$	6.65 ± 0.05	3420 ± 5 (1) ^a	3660 ± 5 (1) ^a	na	37 ± 2	37 ± 5
p_2 TAM $^{3-}$	$\approx 2.6 \pm 0.3^b$	na	3660 ± 5 (2) ^a	na	42 ± 2	72 ± 8
p_2 TAM $^{2-}$	$\approx 1.3 \pm 0.3$	na	≈ 3650 (2) ^a	na	≈ 42	≈ 72
p_2 TAM 0		na	Na	≈ 3750 (2) ^a	≈ 42	≈ 100

^a the values in parenthesis denote the number of phosphono groups.

^b the pK_a value for carboxyl group.

Concentration self broadening of p_1 TAM-D

Concentration-induced line self-broadening of TAM probes is one order of magnitude less than that of nitroxide probes¹ and is not an issue for low concentrations of the p TAM probes. However at high probe concentration line-broadening (see Fig.SI5) is observed.

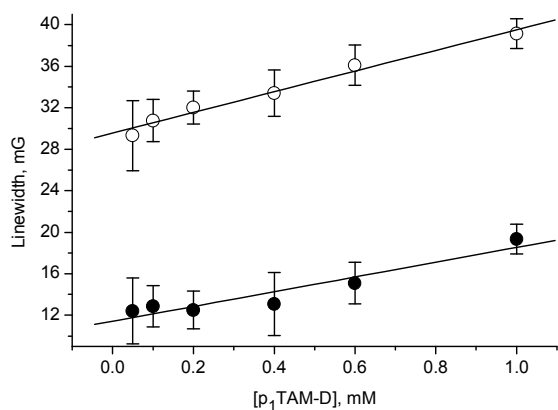


Figure SI5. The concentration dependence of Lorentz linewidths of p_1 TAM $^{3-}$ (\circ) and p_1 TAM $^{4-}$ (\bullet) components of p_1 TAM-D probe. Line represents the best linear fit with the slopes of (10 ± 1) mG/mM and (7 ± 1) mG/mM, correspondingly. L-band EPR spectra were recorded in the presence of 150 mM NaCl and 1mM Na-phosphate buffer under anoxic conditions and temperature of 37 °C.

Partition coefficients for p_1 TAM-D probe

To support high aqueous solubility of p_1 TAM probe, we measured their partition coefficients in octanol/water solutions. The solutions of p_1 TAM-D (200 μ M) in the presence of 0.1 M Na-phosphate buffer at various pHs in the range from 6.0 to 8.0 were vigorously mixed with equal volume of octanol for 5 min and allowed to stand for another 5 min until separation of the phases was completed. The values of the partition coefficient, K_p , were calculated as a ratio of the integral intensities of the EPR spectra of p_1 TAM-D probe in octanol and aqueous phases, correspondingly. The spectrum of p_1 TAM-D probe was found to be below detection limit at these pH values providing an upper limit of K_p value being < 0.001 . For comparison, K_p values for deuterated Finland TAM-D probe was found to be equal to 0.36 ± 0.13 (pH=6), 0.02 ± 0.01 (pH=6.5) and ≤ 0.003 (pH=7). The data support superior aqueous solubility of the phosphonated compound.

Solubility of p_n TAMs at acidic pH

The aggregation of Finland TAM in acidic solutions was previously reported². An introduction of phosphono groups significantly extends the pH range of solubility of the p_n TAM probes (Fig. SI6) apparently due to low pK_a for the phosphonic acid dissociation ($pK_{a1} \approx 1.3$), and therefore maintaining a negatively charged structure at any reasonable pH above pH 3.

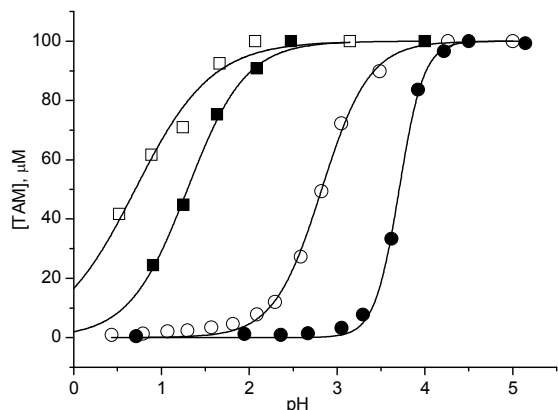


Figure SI6. The dependence of the EPR peak signal intensities of deuterated Finland TAM probe, TAM-D (●, 100 μ M), p_1 TAM-D (○, 100 μ M), p_2 TAM-D (■, 200 μ M), and p_3 TAM-D (□, 200 μ M) on the pH of the sample. Lines represent the best fits using equation $[TAM]_{pH} = [TAM]_0 - [TAM]_0 / (1 + 10^{(pH-pK_{agg})/q})$ yielding $pK_{agg} = 3.7 \pm 0.05$, 2.82 ± 0.05 , 1.30 ± 0.05 and 0.70 ± 0.05 ; and $q = 0.32$, 0.63 , 0.74 and 1 for TAM-D, p_1 TAM-D, p_2 TAM-D, and p_3 TAM-D, correspondingly. The samples were measured in the presence of 1 mM Na-phosphate buffer, 150 mM NaCl and temperature 37 °C.

An exemplified analysis of in vivo L-band EPR spectra of p₁TAM-D probe

Lineshape analysis of the EPR spectrum was performed as previously described³ fitting experimental spectrum by rational approximation of Voigt function given by Hui *et al.*⁴ The independent character of the signal intensities ratio and line broadenings provides dual pH & oxygen functionality, as illustrated below.

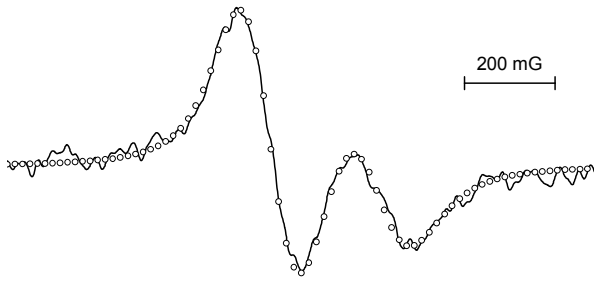


Fig. SI7. L-band EPR spectrum of high-field component of p₁TAM-D probe injected into the mammary gland (0.5 mM, 10 μ l). Circles indicate simulated spectrum yielding the values of pO_2 and pH equal to 54 mmHg and 7.14 pH units, correspondingly.

For the spectrum shown in Fig. SI7, the lineshape analysis yields: $[p_1TAM^{4-}]/[p_1TAM^{3-}] = 1.73$ (which corresponds to pH 7.14); line distance between p₁TAM⁴⁻ and p₁TAM³⁻ lines, 115 mG (which corresponds to 1.4 mM buffer concentration, see Fig. 6B); and Lorentzian linewidths, $L_{tot}(p_1TAM^{4-}) = 46$ mG and $L_{tot}(p_1TAM^{3-}) = 53$ mG. Subtracting from the latter values the Lorentzian linewidths in deoxygenated 1.4 mM phosphate buffer, $L_{buf}(p_1TAM^{4-}) = 21$ mG and $L_{buf}(p_1TAM^{3-}) = 28$ mG (see calibration in Fig. 6A), we obtain oxygen-induced line broadenings, $\Delta L_{ox}(p_1TAM^{4-}) = 25$ mG and $\Delta L_{ox}(p_1TAM^{3-}) = 25$ mG. The latter corresponds to the oxygen partial pressure, $pO_2 = 52$ mmHg (see calibration in Fig. 4). Note that concentration-induced line self-broadening is insignificant at low probe concentrations used. From our previous imaging studies of the membrane-impermeable extracellular probe⁵ we should expect fast p₁TAM-D distribution throughout the tissue of the mammary gland or tumor, therefore final concentration of the probe is about an order lower (50-100 μ M) than the threshold for self-broadening (≈ 400 μ M, Fig. SI5).

Display Report

Analysis Info

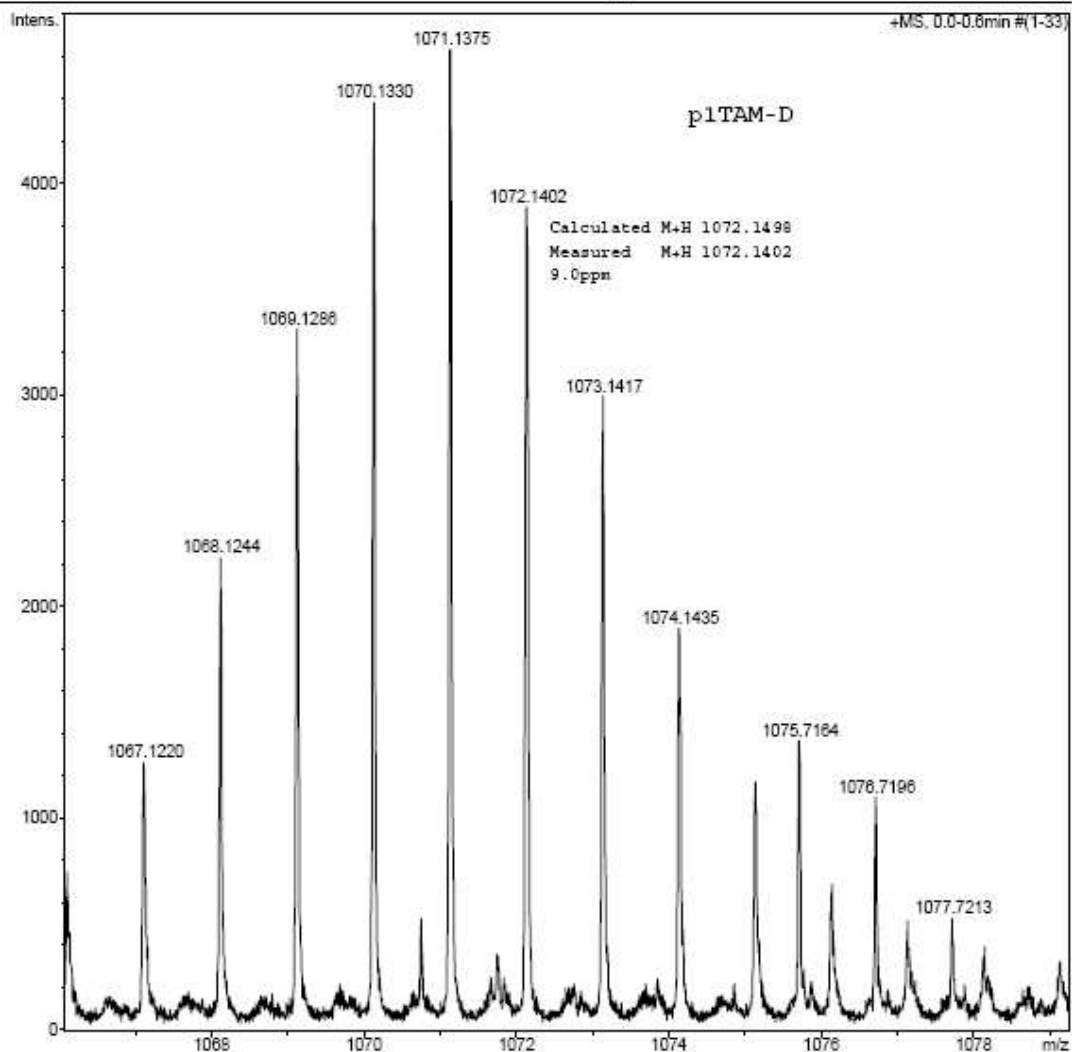
Analysis Name D:\Data\Raw data\X082012B.d
Method pos_tune_mid.m
Sample Name #17271_dFT-P1C2
Comment W/Na Acetate

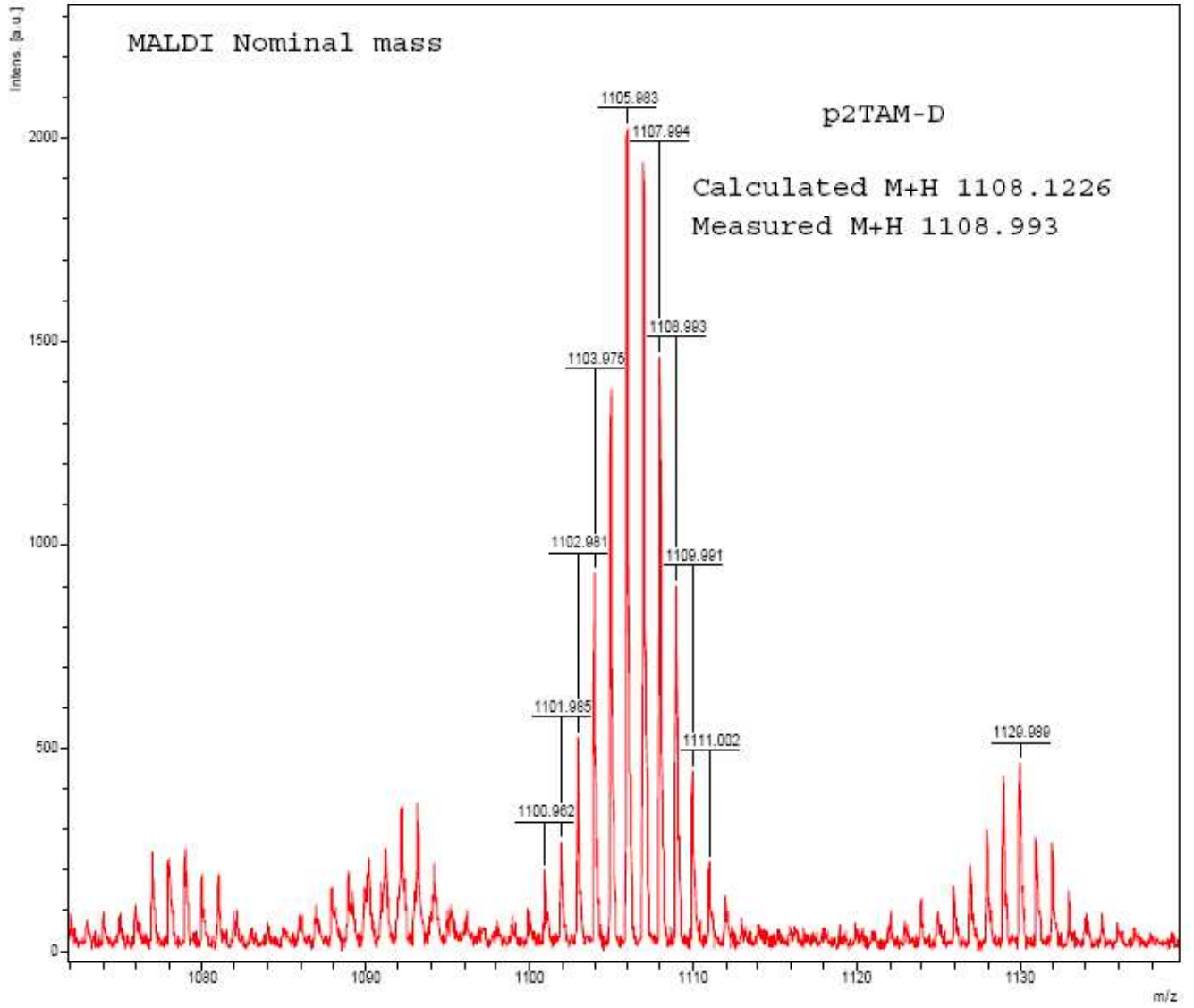
Acquisition Date 8/20/2012 9:55:49 AM

Operator BDAL@DE
Instrument maXis 4G 20196

Acquisition Parameter

Source Type	ESI	Ion Polarity	Positive	Set Nebulizer	0.3 Bar
Focus	Not active	Set Capillary	4500 V	Set Dry Heater	180 °C
Scan Begin	300 m/z	Set End Plate Offset	-500 V	Set Dry Gas	4.0 l/min
Scan End	3000 m/z	Set Collision Cell RF	1200.0 Vpp	Set Divert Valve	Waste





Display Report

Analysis Info

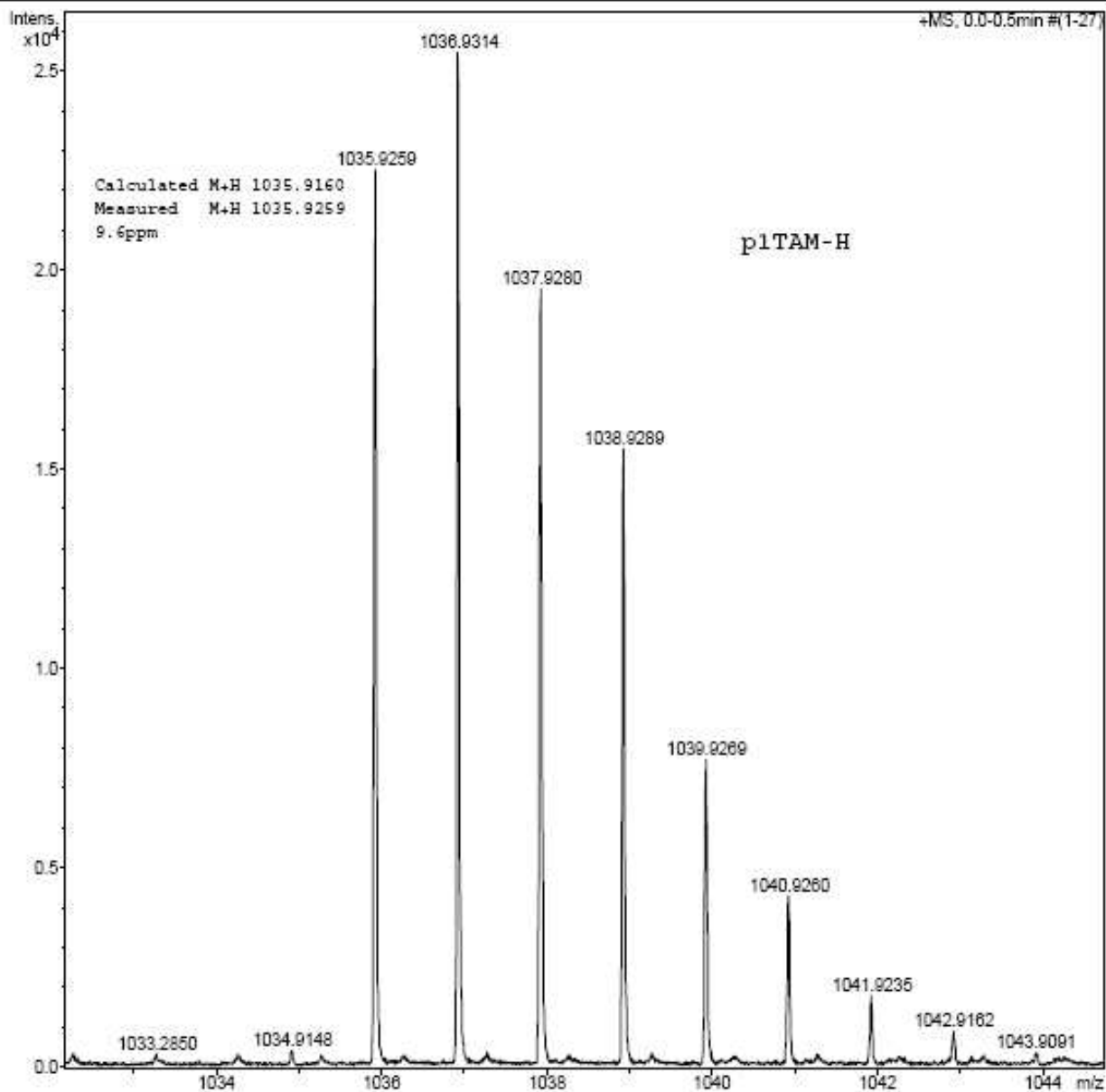
Analysis Name D:\Data\Raw data\X082012C.d
Method pos_tune_mid.m
Sample Name #17271_FT-P1C1
Comment W/Na Acetate

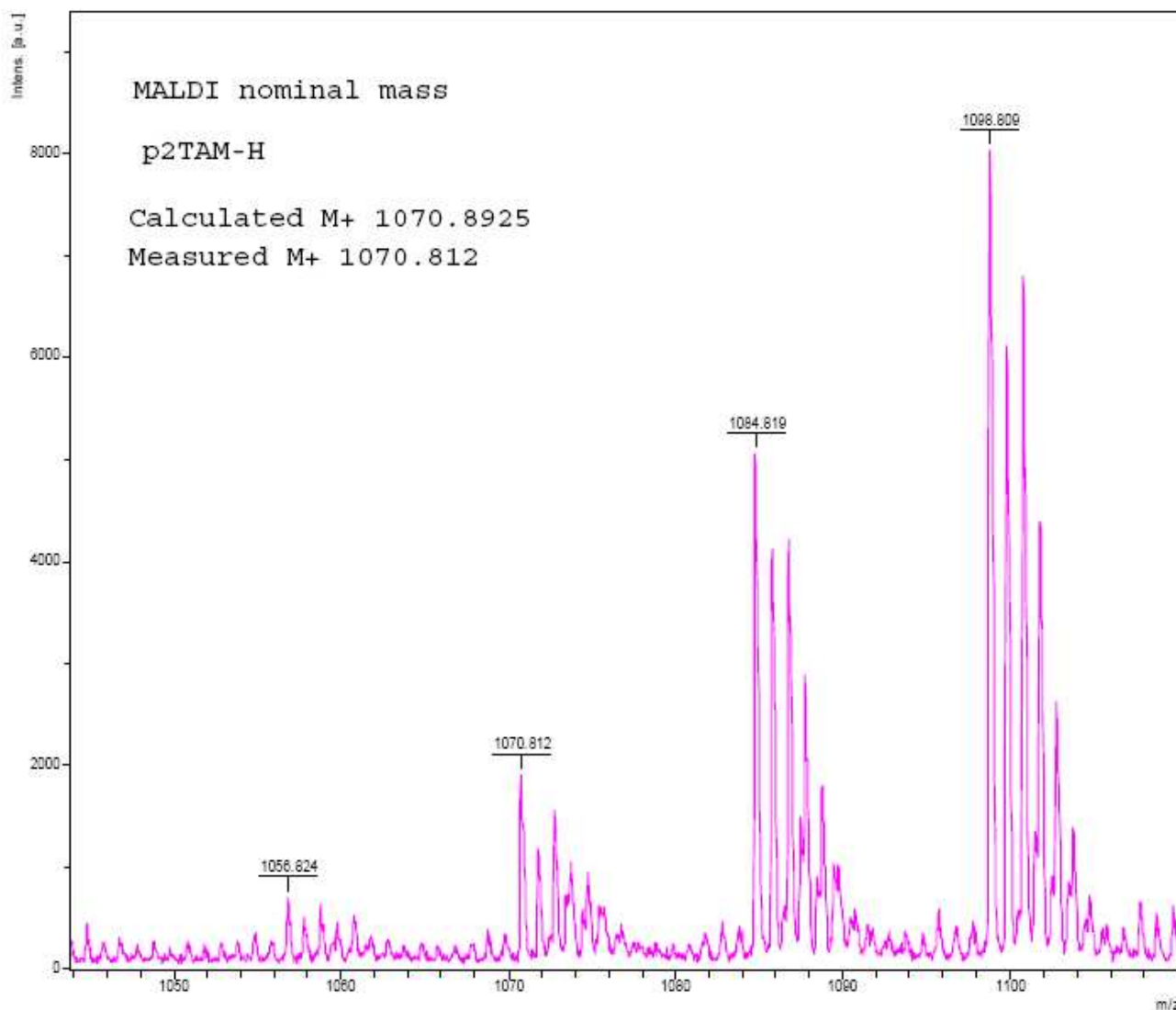
Acquisition Date 8/20/2012 9:59:20 AM

Operator BDAL@DE
Instrument maXis 4G 20196

Acquisition Parameter

Source Type	ESI	Ion Polarity	Positive	Set Nebulizer	0.3 Bar
Focus	Not active	Set Capillary	4500 V	Set Dry Heater	180 °C
Scan Begin	300 m/z	Set End Plate Offset	-500 V	Set Dry Gas	4.0 l/min
Scan End	3000 m/z	Set Collision Cell RF	1200.0 Vpp	Set Divert Valve	Waste





Literature cited

1. Khramtsov, V. V.; Zweier, J. L., Functional in vivo EPR Spectroscopy and Imaging Using Nitroxide and Trityl Radicals. In *Stable Radicals: Fundamentals and Applied Aspects of Odd-Electron Compounds*, Hicks, R., Ed. John Wiley & Sons, Ltd.: Chichester, UK., 2010; pp 537-566.
2. Dhimitruka, I.; Velayutham, M.; Bobko, A. A.; Khramtsov, V. V.; Villamena, F. A.; Hadad, C. M.; Zweier, J. L., Large-scale synthesis of a persistent trityl radical for use in biomedical EPR applications and imaging. *Bioorg Med Chem Lett* **2007**, 17, (24), 6801-5.
3. Komarov, D. A.; Dhimitruka, I.; Kirilyuk, I. A.; Trofimov, D. G.; Grigor'ev, I. A.; Zweier, J. L.; Khramtsov, V. V., Electron paramagnetic resonance monitoring of ischemia-induced myocardial oxygen depletion and acidosis in isolated rat hearts using soluble paramagnetic probes. *Magn Reson Med* **2012**, doi: 10.1002/mrm.23251.
4. Hui, A. K.; Armstrong, B. H.; Wray, A. A., Rapid Computation of Voigt and Complex Error Functions. *Journal of Quantitative Spectroscopy & Radiative Transfer*. **1978**, 19, (5), 509-516.
5. Bobko, A. A.; Eubank, T. D.; Voorhees, J. L.; Efimova, O. V.; Kirilyuk, I. A.; Petryakov, S.; Trofimov, D. G.; Marsh, C. B.; Zweier, J. L.; Grigor'ev, I. A.; Samouilov, A.; Khramtsov, V. V., In vivo monitoring of pH, redox status, and glutathione using L-band EPR for assessment of therapeutic effectiveness in solid tumors. *Magn Reson Med* **2012**, 67, 1827-1836.